Published in: Chemical Engineering and Processing-Process Intensification 150 (2020): 107872

Cavitation bubble dynamics and sonochemiluminescence activity inside sonicated submerged flow tubes

Busra Ekim Sarac, Dwayne Savio Stephens, Julian Eisener[1], Juan Manuel Rosselló, Robert Mettin[*]

Drittes Physikalisches Institut, Georg-August-Universität Göttingen, Friedrich-Hund-Platz 1, 37077 Göttingen, Germany

Abstract

Bubble dynamics and luminol emissions of cavitation in sub-millimeter-sized perfluoroalkoxy alkane (PFA) flow tubes, submerged in an ultrasonic bath reactor, are studied at 27.2 kHz driving frequency. Nucleation of cavitation inside the tubes only takes place via a free interface, realized here in form of an alternating water-air slug flow. High-speed recordings show that cavitation bubbles in the water slugs often develop localized structures in form of clusters or bubble "plugs", and that such structures can be seeded via a single pinch-off from the free interface. Within the structures, bubbles strongly interact and frequently undergo merging or splitting events. Due to the mutual interaction and resulting motion, bubbles often collapse with a fast displacement, suggesting jetting dynamics. Bubble compression ratios are estimated on basis of observed individual bubble dynamics and numerical fitting by a single bubble model that takes the tube wall into account. The resulting peak temperatures around 3500 K allow for dissociation of water vapor. This is in accordance with observed sonochemiluminescence from luminol, originating from active bubble zones in the tubes.

Keywords: sonochemistry; luminol; ultrasound; nucleation; high-speed observations; bubble dynamics

1 present address: Institut für Physik, Otto-von-Guericke-Universität Magdeburg, Universitätsplatz 2, 39106 Magdeburg, Germany

* corresponding author, email address: robert.mettin@phys.uni-goettingen.de (R. Mettin)

1. Introduction

Process intensification (PI), constitutively defined as a continuous processing via flow reactors, is the most promising innovative development in fine-chemical and pharmaceutical industries in the last decades [1]. The overall aim of PI is to improve product quality, control the process precisely, reduce waste, ease the scale up, reduce energy consumption and use the raw material efficiently [2]. One of the recent developments in PI is the use of flow microreactors [3]. Microreactors offer low characteristic length scale, high surface-volume ratio and increase in mixing due to internal circulation; thus, they have the advantage of enhancements of heat and mass transfer coefficients and increase in energy conversion efficiency. Moreover, small volumes can be cost efficient and environment friendly due to the reduction in the size of the equipment, less energy consumption, easier and safer handling of hazardous chemicals, and better controlling ability of reactions taking place at high temperatures and pressures [4].

Innovative research has been focusing on combining microreactors with non-classical, non-contact and sustainable energy sources [5][6]. These include for instance electrostatic fields, microwaves, plasma radiation, and ultrasound. Here we focus on the latter method: irradiation of flow reactors with high frequency acoustic waves, i.e. ultrasound [7].

The general case of chemistry initiated and/or enhanced by ultrasound is termed *sonochemistry*, which is also considered a green and sustainable chemistry [8][9]. The strong ultrasonic driving pressure field forms and expands cavitation bubbles [10][11] in the tension (negative pressure) phase, typically at interfaces or floating weak spots called nuclei. In the subsequent overpressure phase of the field, the bubbles implode and can develop high pressures and temperatures inside of the order of T≈5000 K and P≈1000 bar. The rapid heating can trigger chemical reactions in the gas phase [8][12][13], but also in the liquid phase if liquid enters the collapsing bubble [14] [15].

The chemical effect of cavitation in aqueous environments is often linked to the radical formation in water vapor. Hydrogen atoms and free hydroxyl radicals ($OH^{\bullet}$) are formed as a result of high temperatures and pressures inside the bubble during the last stage of its collapse. The hydroxyl radicals can be detected by visible blue light emission from luminol, termed *sonochemiluminescence (SCL)* [16][17][18]. SCL has to be distinguished from native

sonoluminescence (SL) that is generated in the "hot spot" of the imploding bubble by thermal and plasma radiation [19] [20].

Ultrasound frequencies in sonochemistry range from 20 kHz to several MHz, and amplitudes and operation modes (e.g. pulsed vs. continuous) can be varied. In the framework of microreactors, numerous designs for sonochemistry have been reported in the last decade for different chemical reactions [17] [21] [22]. Among them are: liquid-liquid extraction [21] and gas-liquid mass transfer intensification [23] by a direct contact method of flow tube and Langevin transducer; OH radical formation in a polydimethylsiloxane-based microfluidic reactor in contact with the driving piezo ceramic [17]; handling solid forming reactions by a teflon stack microreactor with an integrated piezoelectric actuator [24] or in a microchannel on top of a Langevin transducer [25]; crystallization through sonication of a flow cell by an integrated piezo ceramic [26]; fabrication of nanoparticle-coated microbubbles through microfluidic channels irradiated by an ultrasonic horn [27]; crystallization of acetylsalicylic acid through milichannels sonicated as well by a horn transducer [28].

As well as various methods to assemble the microreactor exist, different compositions and dimensions of channels, employed according to the reactants and the nature of chemical reaction, have been recently reported. These include glass channels attached to a microscope slide [17], PE/5 channels utilized with an ultrasonic horn [27], PDMS channels via lithography [29], silicon channels via micromachining [18] or PTFE channels in a teflon microreactor [24].

Possibly the most simple way of sonication is the submersion of sound transmissible flow tubes in a larger batch reactor or cleaning bath [30], and we are reporting here on such a setup. Advantages include easy installation, potentially large irradiated volumes and long residence times (i.e. long tube lengths affected by the irradiation), and the possibility of temperature control via the coupling liquid in the bath. Furthermore, the setup can be fully transparent, which is utilized here for direct imaging of cavitation bubbles and for assessment of SCL from luminol. Drawbacks may occur due to larger installation equipment (the bath), frequencies limited to the lower ultrasonic range, lower energy efficiency, or less controlled and unstable operation. The latter point arises since several parameters and conditions of bath and outer (coupling) liquid can affect the energy transfer to the working liquid in the tube, for instance exact fixing position of the tube, filling height, temperature and dissolved gas content of the outer liquid, or dissipation by cavitation therein. These conditions might need additional control

for reliable operation. Still, the submerged tube configuration is a prototypical one that is oftentimes used and that can give general information on properties of cavitation in irradiated tubes or channels. Moreover, modifications and variants of the “simple” submerged tube can alleviate some of the listed downsides in customized configurations, e.g. by employing smaller coupling liquid volumes or higher frequency transducers. From a commercial viewpoint, a submerged tube setup is attractive as a simple and fast test bed for new or modified sonochemical flow processes, and because upscaling in terms of numbering-up of lines in a bath can be relatively cost effective. This property gains in importance facing the general problems of scaling up sonochemical reactions [31] [32] and further motivates a detailed investigation.

In the present study, a perfluoroalkoxy alkane (PFA) tube is submerged into a water-filled ultrasonic bath. PFA is a hydrophobic polymer offering high thermal and chemical resistance. It has also reasonably high flexibility and low bending radius which allow ease of reactor construction. Additionally, PFA provides an opportunity of observing the events taking place inside the channel due to its high transparency. Finally, the acoustic impedance of PFA is close to that of water [33], allowing for nearly transparent sound propagation through the tube walls into the reactive liquid volume.

After a more detailed description of the experimental procedures in Section 2, we discuss the sound field and numerical aspects in Section 3. The main results follow in Section 4: luminol emission measurements, high-speed videography of cavitation bubble structures in the tubes, estimates of bubble collapse compression ratios on basis of numerical fits by a single bubble model, and observation of nucleation events via a free gas/liquid interface. A conclusion is given in Section 5.

2. Experimental part

A schematic drawing of the setup is shown in Figure 1. We employ an in-house made rectangular transparent bath reactor with transparent polycarbonate walls (makrolon, thickness of 6 mm) and open on top. Dimensions of the bath are 140×50×150 mm^3, (l × w × h), and filtered, non-degassed water at room temperature (20°C) as the coupling liquid is filled up to 60 mm height. It is sonicated at 27,2 kHz by one of two piezoceramic Langevin transducers

(Elmasonic, Germany) glued to a steel plate that is forming the bottom wall of the reactor; the other transducer remains unused. The electric signal is provided by a frequency generator (Tektronix AFG 3021, USA) and a power amplifier (E&I Ltd., 1040L, USA) via an in-house built impedance matching box. The acoustic pressure field is mapped with a calibrated hydrophone (Brüel & Kjaer 8103, Denmark) and a digital oscilloscope (Tektronix DPO 4104, USA). Cavitation structures in this reactor under various conditions have been described before in [34]. Here we submerge a PFA tube (BOLA, Germany) of inner diameter $d_i = 1/32''$ (≈ 0.8 mm) and outer diameter $d_o = 1/16''$ (≈ 1.6 mm) from top into the water, whereby the tube undergoes three loops of approximately 50 mm diameter each. The tube loops are fixed parallel in the middle between the long side walls of the reactor and centrally above the driven transducer. This position suggests a maximum of cavitation activity, and no other positions have been investigated in more detail. The tube is connected to a pair of syringe pumps (ProSense, Multi-Phaser^{TM} NE-500, The Netherlands) on the inlet side. The pumps can alternatively supply air or aqueous luminol solution via a T-junction into the tube; the outlet side is open. By switching the pumps, alternating slugs of air and luminol solution of about 1 cm length each are produced inside the submerged tube. During ultrasound operation, the slug lengths and air gaps can change due to mass exchange by droplet ejection and air entrainment, both described below. For the luminol and bubble measurements, the flow is stopped, i.e. the gas/liquid slug distribution in the tube is stationary. SCL measurements are carried out with 0.1 mM luminol solution. Luminol, i.e. 3-aminophthalhydrazide (98%, Fluka, USA) is dissolved in NaOH solution (32 wt.%, Atotech, Germany) and deionized water at room temperature, and pH is adjusted to 11.0. Luminol light emissions are observed by a digital SLR camera (Nikon D700, Japan) in dark room conditions under long exposure (30 s). Cavitation bubbles are visualized by a high-speed camera (Photron, Fastcam SA5, Japan) via a long-distance microscope (K2/SC, Infinity, USA). Illumination is provided by an intense cw white light source (Sumita LS-352A, Japan). Bubbles appear dark in front of a bright background.

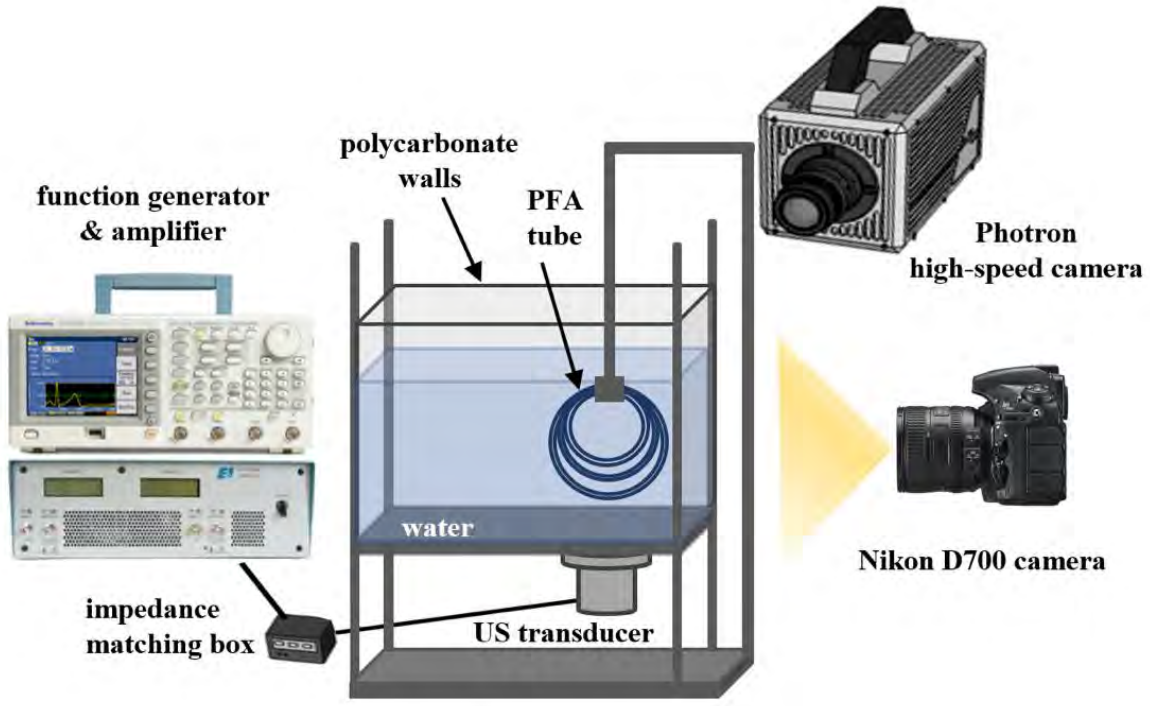

Figure 1: *Schematic drawing of the setup. Three loops of PFA tubing filled with aqueous luminol solution (0.1mM) are submerged in an ultrasonic bath driven at 27.2 kHz and observed by a digital camera. Alternatively, the interior of the tubes is visualized via a long-distance microscope by a high-speed camera with respective illumination.*

3. Sound field and simulations

The ultrasonic field in the resonator develops a standing wave pattern and causes cavitation in the outer (coupling) liquid. Cavitation introduces a higher dissipation rate which actually leads to a certain share of traveling wave in the field [35][36]. For our setup, the acoustic pressure distribution is probed experimentally and simulated numerically for a better characterization of the conditions in the flow channel.

Results from a hydrophone scan of the plane within which the tube is located (recorded in absence of the tube at a delivered electrical power of 65 W) is shown in Figure 2a. The measured rectangular pattern is embedded at the correct position above the transducer in the graph of the cuvette. Due to cavitation, the noise in the measurement is relatively high. The plot shows the color coded amplitude of the fundamental frequency, derived after Fourier transform of the hydrophone time traces from the scan positions. The zones within a distance of 5 mm

from the bottom and the walls could not be accessed due to the hydrophone diameter of nearly 10 mm. It can be seen that a pressure maximum of about 2.5 bar (250 kPa) is found at the bottom in front of the transducer face. Vertically upwards, a low pressure region is passed, and a second maximum zone in the range of 2 bars (200 kPa) occurs. The pressure amplitude in-between the maxima does not completely fall off to zero, indicating a certain traveling wave fraction in the field. The pressure does drop off, as expected, towards the free surface on top and the wall on the side.

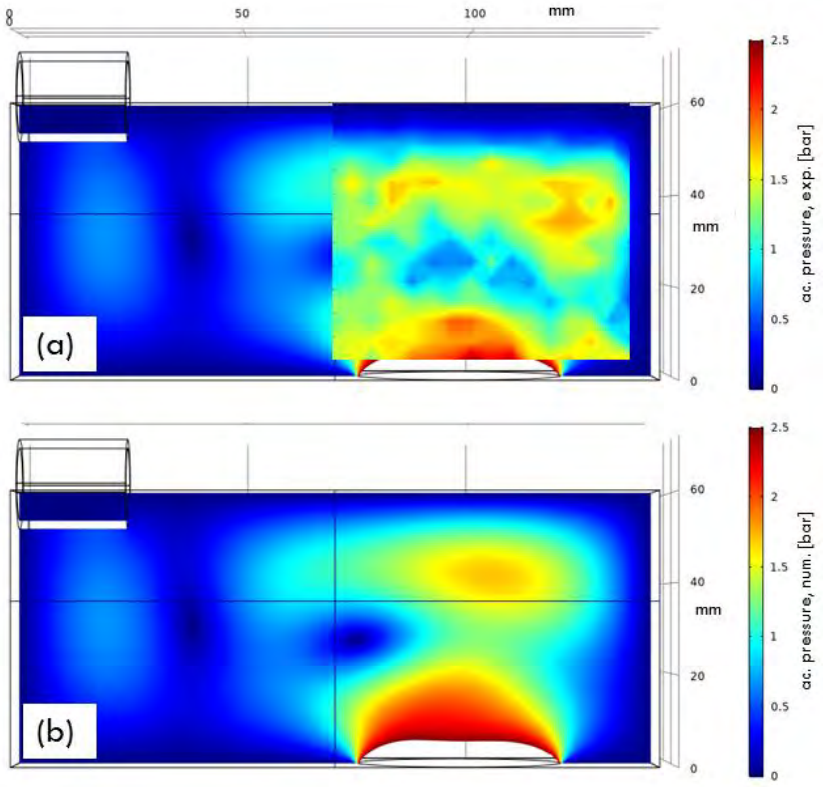

Figure 2: (a) *Measured sound field (color coded pressure amplitude of the fundamental) in the central vertical plane above the transducer (which is positioned below the right bottom). The mapped region is overlaid to a full section of the rectangular reactor with the numerical field in the background. Due to spatial interpolation of the scanned grid data, partially some graphical artefacts of triangular shape appear.* ***(b)*** *Simulated sound field in the reactor (color coded absolute pressure amplitude on a central vertical plane section, homogeneous void fraction* $\beta = 4 \cdot 10^{-7}$*, radiated power 65 W). The color scale is identical in both plots, and it has been limited to 2.5 bar for better contrast. Higher values occur in the simulation directly in front of the transducer, which is indicated by white color.*

The numerical model is based on a modified Helmholtz equation, according to Louisnard [35][36], that takes nonlinear dissipation by homogeneously distributed bubbles into account. In this approach, the bubbles just form passive nuclei below a certain acoustic pressure amplitude threshold, but evolve into strongly dissipating cavitation bubbles beyond that. Parameters are standard values for water and a bubble void fraction of $\beta = 4 \cdot 10^{-7}$ with monodisperse nuclei of equilibrium size $R_0 = 3\mu m$. The model is solved with the finite element software Comsol (Comsol AB, Stockholm, Sweden) in a 3D domain with sound soft boundary conditions at the container walls, bottom plate, and top free surface. The tube is not included. The pressure distribution for a transmitted power of 65 W is shown for the central plane in the resonator in Figure 2b. For the indicated void fraction, the spatial field distribution and as well the maximum pressure values show a fair agreement with the measurement. It can be seen that significant shielding by the bubbles takes place in front of the transducer (where higher pressures occur), leading to rather moderate pressure amplitudes in the bath volume (maxima around 2 bar = 200 kPa). Let us note that for a pure Helmholtz simulation (void fraction of zero, no cavitation bubbles) the wave pattern changes only slightly, but the pressure amplitudes roughly double, which does not coincide with the measurements. On the other hand, the measurement reveals that the antinodal regions are less localized and more extended than suggested by the simulations. Possibly the assumption of a homogeneous bubble field is not true in the real system, and a redistribution of bubbles has to be taken into account to capture this feature.

Based on the measurements and the model, we can assume acoustic driving pressures in the tube of about 200-250 kPa for locations near the bottom maximum, where the optical recordings are conducted. The other parts of the tube loops cross higher and lower pressure regions, mainly between 100 kPa and 200 kPa (compare Figure 3). One would expect that those parts of the tube with driving pressure too low, say below 100 kPa, should not be emitting SCL when containing luminol. This supposes, of course, that disturbances of the field by the tube walls and in particular the air slugs are negligible.

While cavitation bubbles in the outer fluid are free to move when driven by primary Bjerknes forces [11][37] , bubbles inside the tube cannot cross the walls and are thus trapped. However, pressure gradients inside the tubes, both in longitudinal and in transverse direction, can push

the bubbles along the tube or towards the walls. Furthermore, secondary Bjerknes forces that are acting on shorter distances [11][37] will work similarly as in the bulk liquid, with an additional potential attractive mirror-bubble effect near the tube walls [38]. Both transverse primary Bjerknes forces and secondary mirror-bubble Bjerknes forces can lead to preferential bubble locations near the tube walls, and indeed oftentimes clusters appear to be bound to the walls, as illustrated in Section 4.2.

When individual bubble oscillations are resolved sufficiently in the experiment, bubble collapse conditions can be obtained from simulated radius-time dynamics. Employing a numerical bubble model, the bubble equilibrium radius and the local pressure amplitude are fitted to reproduce observed data, as exemplified for trapped stationary bubbles [39]. If the system is unsteady as in typical multibubble systems, the method can still be useful for an estimate. Here we apply a backfolding method of a few observed bubble oscillation periods to a single acoustic period to improve the temporal resolution of the image recordings [40][41]. The dynamics is then fitted by a single spherical bubble model, the Keller-Miksis model [42] [43]. To take into account the presence of the tube walls, we added terms derived by Zudin [44] [45] resulting in the equations

$$R\ddot{R}\left(1-M+\frac{RL}{R_T^2}\right)+\frac{3}{2}\dot{R}^2\left(1-\frac{M}{3}+\frac{4RL}{3R_T^2}\right)=(1+M)\,\frac{p_l}{\rho}+\frac{R}{\rho c}\frac{\mathrm{d}p_l}{\mathrm{d}t} \qquad (1)$$

$$p_l=\left(p_0-p_v+\frac{2\sigma}{R_0}\right)\left(\frac{R_0}{R}\right)^{3\gamma}-\frac{2\sigma}{R}-\frac{4\mu\dot{R}}{R}-\,p_0+p_v-\,p_{\mathrm{ac}}(t) \qquad (2)$$

The model describes the temporal evolution of the bubble radius $R(t)$ of a bubble with equilibrium radius R_0 in a cylindrical rigid tube of radius R_T and length L under driving with $p_{ac}(t)=p_a\sin(2\pi ft)$. Here p_a is the pressure amplitude, and f is the acoustic frequency (27200 Hz). The equation includes compressibility effects by the Mach number of the bubble wall $=\dot{R}/c$, c being the sound velocity in the liquid (1482 m/s). Further parameters are static pressure p_0 (100 kPa), vapor pressure p_v (2.33 kPa), surface tension σ (0.0725 N/m), dynamic viscosity μ (0.001 Ns/m^3), and density of the liquid ρ (998 kg/m^3). The polytropic exponent is set to adiabatic gas compression, i.e. $\gamma=1.4$ for air, and the water properties are valid for a temperature of 20°C. A small channel radius R_T and/or a large channel length L lead to significant influence of the according terms in the model. In particular, one observes a reduction

of the linear resonance frequency and reduced amplitudes of driven oscillations [45]. Large radii and/or short tube lengths, on the other hand, lead to the recovery of the usual bubble dynamics in an infinite liquid.

From the simulations, maximum (R_{max}) and minimum radii (R_{min}) can be identified, and compression ratios R_0/R_{min} can serve as an estimate for peak conditions in the bubble during collapse. Since we use an adiabatic gas compression law, heat conduction, molecule dissociation and ionization, and other energy sinks are neglected. This results in an upper bound for the peak temperatures, and more extended and complex models will somehow lower these figures.

4. Results

4.1 Luminol emissions

For sonicating the tube being fully filled with liquid, we do not obtain any luminol signal, and neither do we observe bubbles in the tubes. This is in accordance with other reports on cavitation in small channels (e.g. Tandiono et al. for PDMA channels of 20 µm height and sonicated directly via the substrate at 100 kHz [17]). Here it shows that also in the larger tubes no nucleation of cavitation bubbles occurs under completely filled conditions. Both luminol emission and visual bubbles, however, do appear for alternate filling with liquid and air. For imaging, the flow has been stopped to improve contrast since the SCL emissions were generally quite low. Then, the non-moving slugs of aqueous luminol solution partly show weak emission of the characteristic blue light, indicating production of OH radicals by cavitation [16].

Two examples for recorded SCL signals from different runs are shown in Figure 3 where the tube position and the measured sound field are included as reference as well. For Figures 3b and 3c, the blue SCL emissions have been extracted from the raw images (30 s exposure) and then superimposed to the color mapped measured sound field (compare Figure 2a). The emissions clearly retrace the shape of the tube loops. Gaps in the emission along the tube can occur due to an air slug, missing nucleation in the specific water slug (see Section 4.4), insufficient driving pressure for cavitation or chemical reactions taking place, or a signal too low to be detected during exposure. Since the slug lengths are somehow changing during

sonication, there occur also emitting regions or gaps longer or shorter than about 1 cm. Furthermore, some regions show stronger localized signals (brighter spots). This is in accordance to the localized bubble structures inside the slugs, as described in the following Section. The correspondence of SCL regions and higher pressure zones is fair, although we do not observe a full correlation. While the emissions are indeed low or absent in the low pressure region to the lower right, there are on the other hand clear signals from the left part of the low pressure valley. Also some upper parts of the loops, close to the free surface and apparently driven only weakly, show SCL emission.

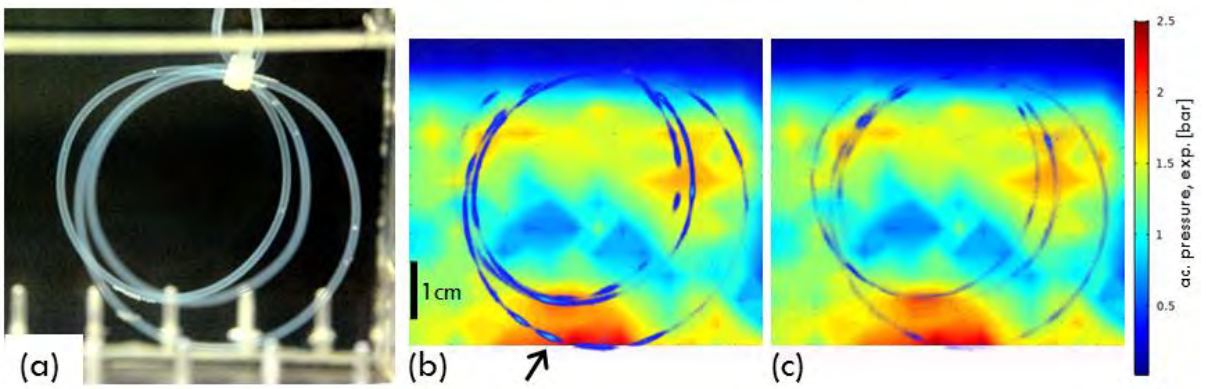

Figure 3: (a) *Bright image of the tube loops in the reactor. Vertical bars at the bottom are screws in the transparent walls. The horizontal bright line in the upper part is the water surface.* ***(b, c)*** *Imaged luminol emissions and their relation to the measured sound field: Dark room exposures (30 s) for two different runs are overlaid onto the color map of the measured acoustic pressure amplitude distribution. The round dark blue structures are the SCL emissions, retracing the tube loops. The arrow in (b) indicates the approximate position where the optical high-speed images from Figure 4 are taken. A scale bar indicates the dimensions.*

Potentially, the presence of gas slugs is perturbing the field significantly due to reflections, and such effects have to be taken into account. This could also explain differences of emissions between Figure 3b and 3c. Interestingly, the cavitation phenomena in the tubes generally show variations depending on liquid slug length and slug spacing (i.e., gas pocket length). This variability has also been observed before [46], and it is subject of future studies. Preliminary results from Comsol simulations suggest potential acoustic resonance effects along the liquid slugs that might explain cavitation activity in spite of lower outer driving field.

4.2 Bubble structures

Recordings of cavitation bubbles have been done in a section of the tube approximately 5 mm above the transducer (the lowest central left tube part, marked by an arrow in Figure 3b) with stopped flow. Very similar bubble patterns are observed under slow flow conditions (several mm/s), but the dependence of cavitation on the flow speed has not been investigated in more detail yet. The bubbles appear quite intermittent and in a certain variety, i.e., cavitation activity is far from homogeneous in time and space. Figure 4 illustrates prototypical bubble ensembles, all observed within a total recording time of about one second. In particular, we see many times wall attached clusters in form of a roughly half spherical aggregate at the bottom or top of the tube (Figure 4a, b). Other frequent structures are "plugs" of bubbles, i.e., a roughly rectangular region extending from top to bottom of the tube and with rather sharp limits at the sides (Figure 4c, d and e, f). It remains unclear if the plugs are similar to the wall attached clusters, but just seen from below or from top (i.e., attached to the front or back wall of the tube). Both structure types show a pronounced confinement of bubbles in longitudinal tube direction. The boundaries to the neighbored, nearly bubble free regions occur somehow sharper for plugs, which might hint to a structure actually different from a wall cluster. Less confined structures appear as well, and they form streamers that cross larger longitudinal sectors (Figure 4g, h), or appear as fully dispersed bubble fields (Figure 4i, k). Inside the confined structures, cavitation bubbles interact strongly: merging or splitting take place every few acoustic cycles, sometimes during each oscillation period. Accordingly, the bubbles move, and frequently a collapse "jump" appears, at times with a resolved jetting event. In Figure 4l, m displacement and jetting can be discerned (marked by arrows; due to the long exposure time the bubble silhouette over half a period is visible as a grey shade). The rapid displacement and the merging events prevent oftentimes a clear re-identification of an individual bubble after collapse, even more since many bubbles disappear from the image during the collapse phase due to limited spatial resolution (about 5 μm/pixel). Within the more dispersed structures, bubbles show less frequent interaction, as expected from the larger inter-bubble distances. Still, collision events take place frequently, i.e., every few acoustic cycles. The numbers of identifiable and resolved bubbles in the structures range from about 30 – 200, but it has to be noted that the amount of visible bubbles within one structure is variable during the oscillation period. Few bubbles can be seen during the collapse phase (for limited resolution), and the highest number of bubbles occurs somehow between minimum and maximum expansion. At the fully expanded state, again the bubble number is

decreased, partly only apparently due to optical overlap and shielding, partly due to true merging (compare also Fernandez Rivas et al. [47] for this phenomenon). To demonstrate the variability of bubble sizes and numbers, all structures in Figure 4 are shown in a nearly collapsed phase (first frame) and in the subsequent expansion phase (second frame). The void fraction in the collapsed cluster of Figure 4e is roughly estimated to about $2.5 \cdot 10^{-4}$, and it increases 100-fold to about $2.5 \cdot 10^{-2}$ in the expansion phase (Figure 4f). These numbers appear typical for the localized structures.

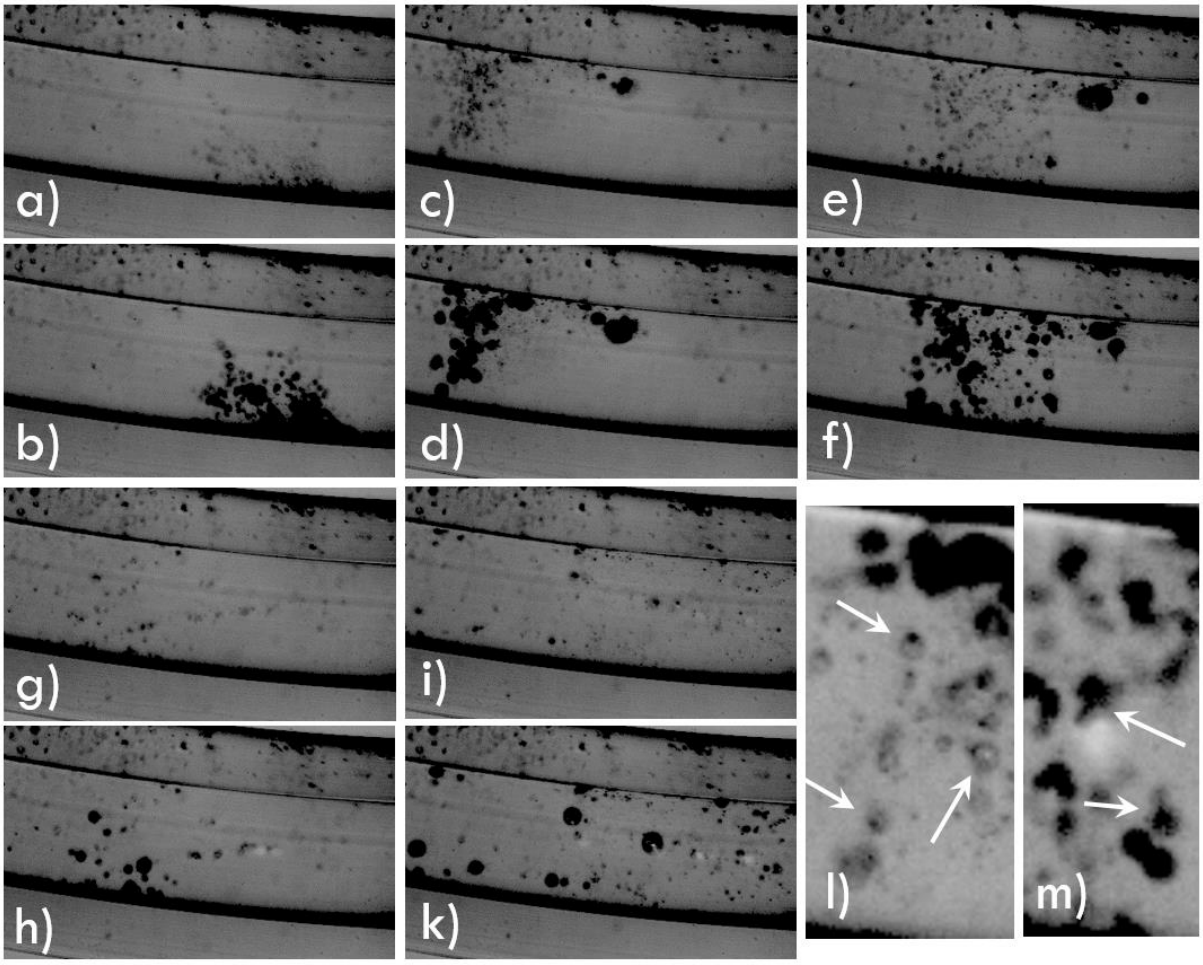

Figure 4: *Different cavitation bubble structures in the tube, all shown in a nearly collapsed phase and the subsequent phase near maximum expansion: Wall attached cluster (a, b); narrow plug (c, d); wider plug (e ,f); streamer (g, h); disperse (i, k). Displacement and jetting of collapsing bubbles are marked in frames l) and m). Recording with 20000 fps, exposure time 50 µs, frame heights ca. 1.5 mm in a) to k) and ca. 0.8 mm in l) and m). See also Movie1.avi in the supplementary material.*

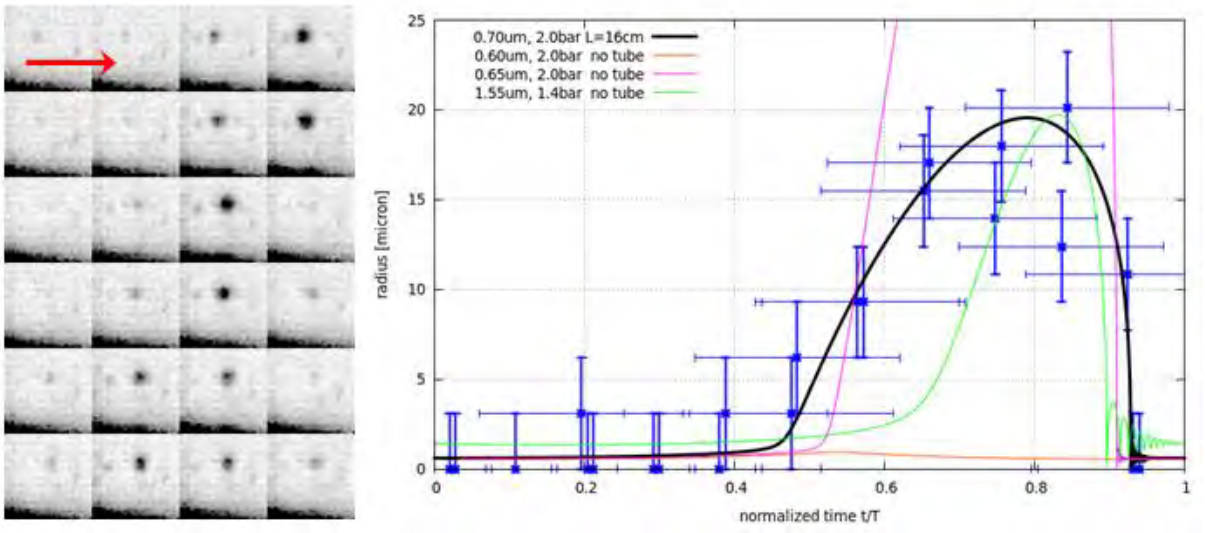

Figure 5: *A single bubble at the edge of a cluster inside the tube.* ***Left:*** *Image series showing the nearly stationary dynamics over 24 frames, corresponding to 6 driving periods (sequence from top left in direction of arrow, row by row; recording at 100 kfps, 10 µs exposure time, frame width 192 µm).* ***Right:*** *Reconstructed radius-time dynamics (experimental radius data with error bars, back-folded onto one driving period* $T = 1/f$*). Different cases of modeled bubble oscillations are shown by colors (see text). The best fit for the nominal pressure amplitude of* p_a *= 2 bar (200 kPa) is found for* R_0 *= 0.7 µm in a tube of length L = 16 cm (thick black line).*

4.3 Bubble dynamics reconstruction

Since the single-bubble model that is employed for the radius-time reconstruction is based on spherical and stationary oscillation, one should apply it to a bubble being more or less isolated for a few cycles. However, such bubbles are scarce within the structures, and not many test bubbles could be identified. Here we show a representative bubble at the border of a slim "plug", recorded at 100 kfps. Figure 5 shows on the left the section of the recording used, and the right plot presents the measured radius-time data points folded back onto a single driving period, supposing a periodic oscillation. The periodicity is apparently not perfectly given since not all the data points fall on a single curve, but one can coherently recognize a phase of small bubble size until $t/T \approx 0.4$, an expansion phase for $0.4 < t/T < 0.6$, and collapse at about $t/T \approx 0.9$. Since the equilibrium radius should correspond roughly to the bubble size before expansion, one gets $R_0 < 3.5$ µm. The maximum radius amounts to $R_{max} \approx 20$ µm, which

already indicates an expansion ratio R_{max}/R_0 larger than 6, and therefore strong collapses. Employing the model equations (1), (2) with a driving pressure amplitude of 200 kPa, which is suggested by the measurements of the sound field, one obtains a quite good fit for $R_0 = 0.7$ µm, $R_T = 0.4$ mm, and $L = 16$ cm. The resulting radius-time curve is superimposed to the data in Figure 5 with a suitable temporal shift to adjust the unknown phase (thick black line). The modeled bubble collapses down to $R_{min} = 0.085$ µm which translates into a maximum gas compression ratio $\alpha = R_0/R_{min} \approx 8$. From this figure one derives a peak temperature via the adiabatic law $T_{max} = T_0\alpha^{3(\gamma-1)}$ with the ambient temperature $T_0 = 293$ K. Here we find $T_{max} \approx 3500$ K.

Let us note that a successful bubble dynamics fit remains difficult without taking the tube into account. Trials to reproduce the data with the standard Keller-Miksis model ($L = 0$) for $\mathrm{p_a} = 200$ kPa lead to very sensitive parameters close to the Blake threshold ("giant response", see e.g. [43]) where slight variation of R_0 leads to either too small or too large values of R_{max}. This is illustrated in Figure 5 by inclusion of the curves for $R_0 = 0.60$ µm (brown) and $R_0 = 0.65$ µm (pink; the maximum is lying out of the plot region). Furthermore, if a lower driving pressure is assumed to meet R_{max}, the resulting expansion phase is much too short. For demonstration, the curve for $R_0 = 1.55$ µm and $\mathrm{p_a} = 140$ kPa is included as well in the plot (green) which well hits R_{max}, but cannot reproduce the extended expansion. We have also to note that for the good fit, while the tube radius is fixed according to the experiment, the tube length parameter L has to be chosen larger than a typical liquid slug length (about 1 cm). Otherwise R_{max} comes out too large again. Possibly an influence of the neighbored cluster bubbles needs to be taken into account as well, which can have similar effects as the tube wall [48].

As stated above, the adiabatically heated bubble peak temperature of 3500 K represents rather an upper bound, but the true value should well be sufficient to dissociate trapped water vapor molecules to a substantial part into H and OH radicals [13] [49] [50]. Other bubbles in the structures show similar maximum and minimum radii as the particular bubble fitted here, which is why we conclude that luminol emission is consistent with the observed bubble dynamics in the clusters. Thus the localized bubble structures can unambiguously be identified as the sources of OH radicals and blue SCL light.

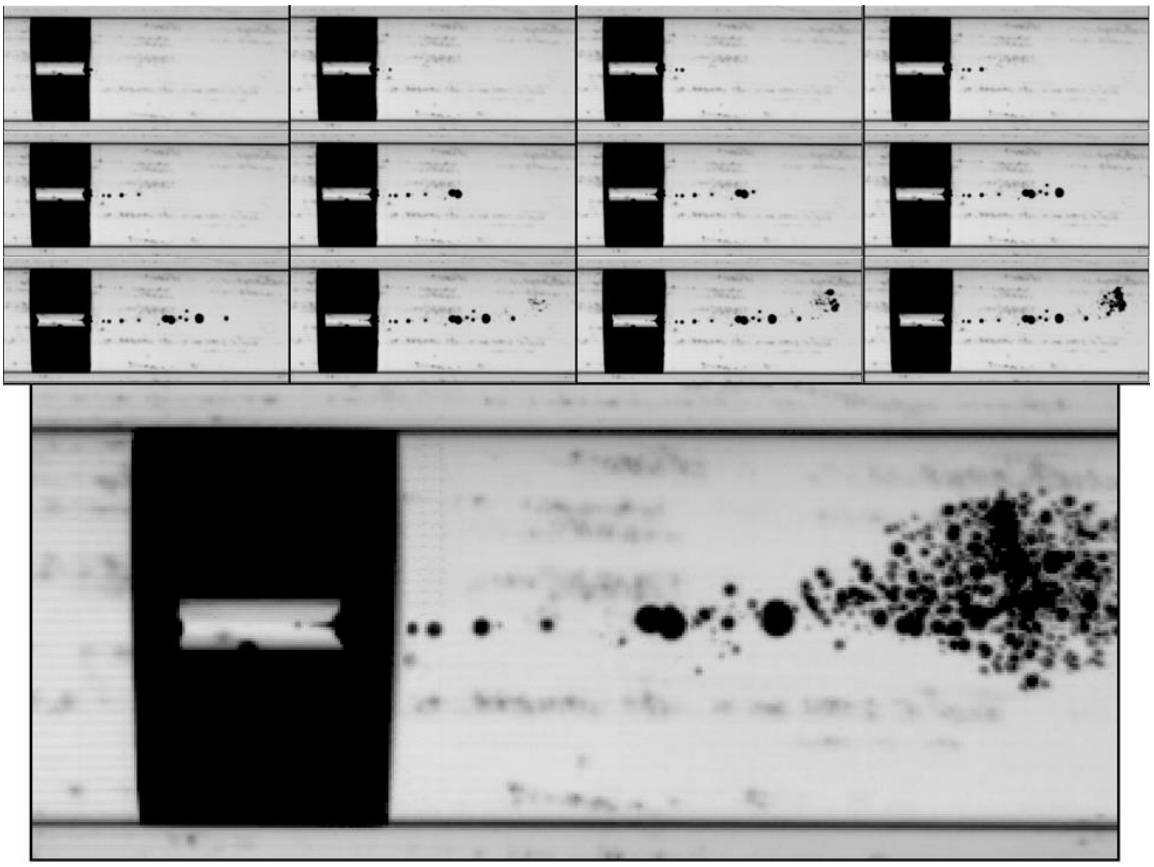

Figure 6: *Bubble nucleation at the free interface between gas and air slug: The upper picture series shows in form of cumulative images the path of the entering bubble (all former bubble positions stay visible in subsequent frames). The lower image shows a later stage when the bubble has transformed into a cluster (recording at 27500 fps, exposure time 1 µs, frame height 1 mm). See also Movie2.avi in the supplementary material.*

4.4 Bubble nucleation

The origin of cavitation bubble structures in the PFA tube is apparently based on nucleation events that occur at the free interface between liquid and gas slugs, since in the absence of the gas slugs, no cavitation is detected. Recordings in a setup virtually identical to Figure 1, but with horizontally aligned tubes in a holder frame, have captured individual bubble entrainments into the liquid from the gas. One such event is shown in Figure 6. The interface forms bulges and indentations, most likely connected to acoustically driven capillary waves [51]. Once seeded, the entering single bubble travels away from the interface and develops into a cluster

by splitting and thus multiplying the bubble number. Calculation of the wavelength $\lambda_c \approx \sqrt[3]{\frac{2\pi\sigma}{\rho f_c^2}}$ [52] with the parameters for water and a Faraday capillary wave frequency of half the driving frequency, $f_c = f/2$, leads to $\lambda_c \approx$ 135 µm. The observed bulge width in the center of the interface shown in Figure 6 amounts to about 85 µm, which is somewhat larger than the expected $\lambda_c/2 \approx 67.5$ µm. Probably, an influence of the spherical boundary conditions for the free surface inside the tube should be taken into account, leading to a surface oscillation mode of a wavelength different to the case of an infinite interface. The buildup of the bulge quite centrally on the axis of the tube gives further support for a symmetric mode oscillation of the interface here.

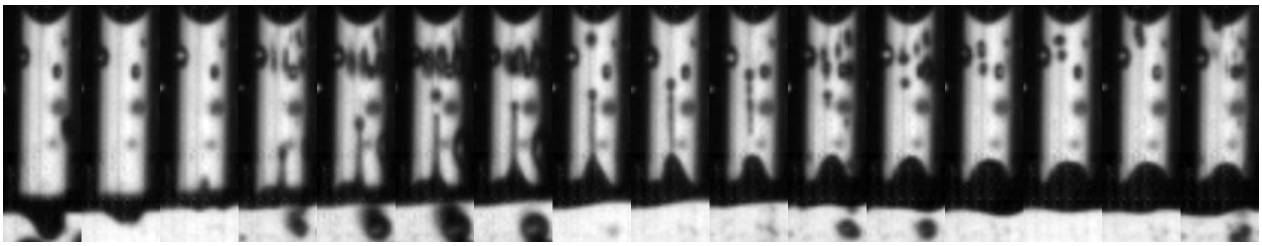

Figure 7: *Droplet ejection at the interface from water (lower part of image) into air (upper part). Recording at 150000 fps, exposure 2 µs, frame width approx. 200 µm, images turned 90° as compared to Figure 6. The bulge develops a thin jet that separates and disintegrates into drops. The dark structure below the interface after the third frame is a freshly created bubble that afterwards undergoes volume oscillations in the ultrasonic field. See also Movie3.avi in the supplementary material.*

On the other side of the free interface, droplets can be ejected into the gas volume by essentially the same capillary wave dynamics. In Figure 7 such a case is presented where a central liquid jet is produced that disintegrates into drops. The first drop has a radius of about 11 µm (resulting in a volume of 5.6 pl). Its velocity reaches about 9 m/s, and the subsequent train of droplets flies with roughly 3 m/s into the gas slug. Ejected drops can hit the tube wall or the opposite interface of the next liquid slug. The drop ejection by capillary waves observed here appears similar to ultrasonic atomization at open free surfaces [53]. The atomization at inner free surfaces has also been observed to be responsible for the wetting of gas filled holes under

ultrasound irradiation [54]. In our experiment, it seems that the slugs can change their length on a longer time scale due to the mass transfer by ejected drops and entering bubbles. From the image series in Figure 7 it appears that in this case the droplet ejection is also accompanied by a bubble creation. This is, however, not always happening. Still, drop ejection and bubble nucleation could be connected in some cases.

5. Discussion and conclusion

We have investigated cavitation in 1/32" inner diameter PFA flow tubes submerged in an ultrasonic bath, running at 27.2 kHz. Nucleation can only be observed under liquid/gas slug flow conditions where a free interface is present, which is in accordance to previous observations in directly irradiated microchannels by Tandiono et al. [17] [51]. In contrast to Tandiono's work, here we deal with much larger liquid volumes and larger gas-liquid interfaces, the cross sections of the flow being 50 times larger (i.e., rather "milli" than "micro"channels). Furthermore, due to the flat geometry of Tandiono's microchannels (20 µm height and 500 µm width), the bubbles are mainly cylindrical, i.e., in contact with the upper and lower walls. This confines the bubble oscillation and bubble translation to essentially two dimensions, leading to several different effects as compared to our larger and round channels. In particular, in the flat channels the bubbles form a type of foam plug in expanded state, while in the larger diameter channels they can move rather freely and arrange in three-dimensional clusters. Accordingly, Tandiono reports on SCL being bounded to regions near the liquid/gas interfaces, while in our setup SCL can spread over a complete water slug, once bubbles are seeded. Furthermore, the irradiation of the flat microchannels was done at 100 kHz via the substrate, while we sonicate at 27.2 kHz via the coupling liquid. Still, nucleation happens only at the interface, indicating that nuclei are sparse or absent in the bulk liquid volume and at the tube walls. We have imaged such nucleation events taking place by single bubble entrainment, induced by acoustically driven interface deformations, probably capillary waves. As well, droplets can be ejected into the gas phase via disintegration of liquid jets, apparently as well triggered by capillary waves. Bubble entrainment and drop ejection can happen simultaneously, as shown in one such event.

Once nucleated, single entrained bubbles can develop into a larger bubble cluster. Generally, cavitation bubbles within the tube frequently form localized structures like clusters or plugs,

i.e., confined small sections of the tube with cavitation activity. Often clusters seem bound to the channel wall, which might be caused by primary Bjerknes forces from the irradiated field and by secondary Bjerknes forces via a mirror bubble effect.

From individual bubble dynamics in a bubble structure, we estimate via numerical fitting the bubble equilibrium radius and the peak temperature. The best fit is found when taking the tube walls into account. The obtained peak value of 3500 K should be sufficient for a significant amount of hydrolysis and OH radical production of the water vapor trapped during collapse [55]. This is consistent with observations of SCL from luminol in the submerged sonicated tubes, indicating the presence of OH radicals. Detailed evaluation and statistics of the emerging bubble structures would allow for estimation of bubble numbers and – together with collapse ratios – to estimate sonochemical activity. Such results might be contrasted to photon counting measures of SCL or other sonochemical dosimetrics in future investigations.

In essence, we have confirmed that cavitation in flow tubes submerged in an ultrasonic bath can serve as a simple sonochemical flow reactor if bubble nucleation is facilitated. Apart from free interfaces, also other types of inhomogeneities might potentially be considered for bubble seeding [22]. The sonication of the tube via a coupling liquid might limit the reachable pressure amplitudes, in particular if cavitation and shielding in the coupling liquid occur. Furthermore, standing wave structures in the bath could inhibit cavitation activity in the full tube volume and thus shorten effective residence times. However, the presence of gas slugs in the tube might disturb the sound field and alleviate this effect. Future studies will focus on a better control of tube positions and field distribution, on more details of multi-bubble dynamics in the confined clusters, and on different coupling liquids. Identification, control and optimization of the problematic points of submerged tube setups might finally contribute to upscaling and numbering-up of sonochemical flow processes.

Acknowledgement

The authors would like to thank the mechanical and electrical workshops at Drittes Physikalisches Institut for their support. The research leading to these results has received funding from the European Union's Horizon 2020 research and innovation programme under the Marie Skłodowska-Curie grant agreement No 721290 (MSCA-ETN COSMIC). This

publication reflects only the author's view, exempting the Community from any liability. Project website: https://cosmic-etn.eu/.

References

[1] T. Van Gerven and A. Stankiewicz, "Structure, energy, synergy, time-the fundamentals of process intensification," *Ind. Eng. Chem. Res.*, vol. 48, no. 5, pp. 2465–2474, 2009.

[2] C. Ramshaw, "Process Intensification: a game for n players," *Chem. Eng.*, vol. 416, pp. 30–33, 1985.

[3] V. Hessel, "Process windows - gate to maximizing process intensification via flow chemistry," *Chem. Eng. Technol.*, vol. 32, no. 11, pp. 1655–1681, 2009.

[4] D. Fernandez Rivas and S. Kuhn, "Synergy of Microfluidics and Ultrasound: Process Intensification Challenges and Opportunities," *Top. Curr. Chem.*, vol. 374, no. 5, pp. 1–30, 2016.

[5] R. van Eldik and C. D. Hubbard, *Chemistry Under Extreme and Non-Classical Conditions*. John Wiley & Sons, 1996.

[6] A. Stankiewicz, "Energy matters: alternative sources and forms of energy for intensification of chemical and biochemical processes," *Chem. Eng. Res. Des.*, vol. 84, no. A7, pp. 511–521, 2006.

[7] K. S. Suslick, "Ultrasound: Its Chemical, Physical, and Biological Effects," *J. Acoust. Soc. Am.*, vol. 87, no. 919, 1990.

[8] K. S. Suslick, "Sonochemistry," *Science*, vol. 247, no. 4949, pp. 1439–1445, 1990.

[9] T. J. Mason, "Sonochemistry and the environment - Providing a 'green' link between chemistry, physics and engineering," *Ultrason. Sonochem.*, vol. 14, no. 4, pp. 476–483, 2007.

[10] F. R. Young, *Cavitation*. McGraw-Hill, 1989.

[11] T. Leighton, *The Acoustic Bubble*. Academic Press, 1994.

[12] D. Lohse, “Sonoluminescence: Cavitation hits up,” *Nature*, vol. 434, no. 7029, pp. 33–34, 2005.

[13] P. Riesz, D. Berdahl, and C. L. Christman, “Free radical generation by ultrasound in aqueous and nonaqueous solutions,” *Environ. Health Perspect.*, vol. VOL. 64, pp. 233–252, 1985.

[14] H. Xu, N. C. Eddingsaas, and K. S. Suslick, “Spatial separation of cavitating bubble populations: The nanodroplet injection model,” *J. Am. Chem. Soc.*, vol. 131, no. 17, pp. 6060–6061, 2009.

[15] A. Thiemann, F. Holsteyns, C. Cairós, and R. Mettin, “Sonoluminescence and dynamics of cavitation bubble populations in sulfuric acid,” *Ultrason. Sonochem.*, vol. 34, pp. 663–676, 2017.

[16] H. N. McMurray and B. P. Wilson, “Mechanistic and spatial study of ultrasonically induced luminol chemiluminescence,” *J. Phys. Chem. A*, vol. 103, no. 20, pp. 3955–3962, 1999.

[17] Tandiono, S.-W. Ohl, D. S. W. Ow, E. Klaseboer, V. V. Wong, R. Dumke, and C.-D. Ohl, “Sonochemistry and sonoluminescence in microfluidics,” *Proc. Natl. Acad. Sci. U. S. A.*, vol. 108, no. 15, pp. 5996–5998, 2011.

[18] D. Fernandez Rivas, P. Cintas, and H. J. G. E. Gardeniers, “Merging microfluidics and sonochemistry: Towards greener and more efficient micro-sono-reactors,” *Chem. Commun.*, vol. 48, no. 89, pp. 10935–10947, 2012.

[19] L. A. Crum, “Resource Paper: Sonoluminescence,” *J. Acoust. Soc. Am.*, vol. 138, no. 4, pp. 2181–2205, 2015.

[20] R. Pflieger, S. I. Nikitenko, C. Cairós, and R. Mettin, *Characterization of Cavitation Bubbles and Sonoluminescence*. Springer International Publishing, 2019.

[21] J. J. John, S. Kuhn, L. Braeken, and T. Van Gerven, “Ultrasound assisted liquid-liquid extraction in microchannels-A direct contact method,” *Chem. Eng. Process. Process Intensif.*, vol. 102, pp. 37–46, 2016.

[22] D. Fernandez Rivas, A. Prosperetti, A. G. Zijlstra, D. Lohse, and H. J. G. E. Gardeniers, "Efficient sonochemistry through microbubbles generated with micromachined surfaces," *Angew. Chemie - Int. Ed.*, vol. 49, no. 50, pp. 9699–9701, 2010.

[23] Z. Dong, C. Yao, X. Zhang, J. Xu, G. Chen, Y. Zhao, Q. Yuan, "A high-power ultrasonic microreactor and its application in gas-liquid mass transfer intensification," *Lab Chip*, vol. 15, no. 4, pp. 1145–1152, 2015.

[24] S. Kuhn, T. Noël, L. Gu, P. L. Heider, and K. F. Jensen, "A Teflon microreactor with integrated piezoelectric actuator to handle solid forming reactions," *Lab Chip*, vol. 11, no. 15, pp. 2488–2492, 2011.

[25] C. Delacour, C. Lutz, and S. Kuhn, "Pulsed ultrasound for temperature control and clogging prevention in micro-reactors," *Ultrason. Sonochem.*, vol. 55, pp. 67–74, 2019.

[26] R. Jamshidi, D. Rossi, N. Saffari, A. Gavriilidis, and L. Mazzei, "Investigation of the Effect of Ultrasound Parameters on Continuous Sonocrystallization in a Millifluidic Device," *Cryst. Growth Des.*, vol. 16, no. 8, pp. 4607–4619, 2016.

[27] H. A. Chen , H., Li, J., Zhou, W., Pelan, E. G., Stoyanov, S D., Anaudov, L. N., Stone, "Sonication−Microfluidics for Fabrication of Nanoparticle-Stabilized Microbubbles," *Langmuir*, vol. 30, pp. 4262–4266, 2014.

[28] G. Valitov, R. Jamshidi, D. Rossi, A. Gavriilidis, and L. Mazzei, "Effect of acoustic streaming on continuous flow sonocrystallization in millifluidic channels," *Chem. Eng. J.*, vol. 379, p. 122221, 2020.

[29] Q. Tseng, A. M. Lomonosov, E. E. M. Furlong, and C. A. Merten, "Fragmentation of DNA in a sub-microliter microfluidic sonication device," *Lab Chip*, vol. 12, no. 22, pp. 4677–4682, 2012.

[30] M. Oelgemoeller, "Highlights of Photochemical Reactions in Microflow Reactors," *Chem. Eng. Technol.*, vol. 35, no. 7, pp. 1144–1152, 2012.

[31] P. R. Gogate, V. S. Sutkar, and A. B. Pandit, "Sonochemical reactors: Important design and scale up considerations with a special emphasis on heterogeneous systems," *Chem. Eng. J.*, vol. 166, no. 3, pp. 1066–1082, 2011.

[32] J.-M. Lévêque, G. Cravotto, F. Delattre, and P. Cintas, “Scaling-Up Enabling the Full Potential of Industrial Applications of Ultrasound and Hydrodynamic Cavitation,” in *Organic Sonochemistry: Challenges and Perspectives for the 21st Century*, Cham: Springer International Publishing, 2018, pp. 113–123.

[33] M. I. Gutierrez, S. A. Lopez-Haro, A. Vera, and L. Leija, “Experimental Verification of Modeled Thermal Distribution Produced by a Piston Source in Physiotherapy Ultrasound,” *Biomed Res. Int.*, vol. 2016, 2016.

[34] F. Reuter, S. Lesnik, K. Ayaz-Bustami, G. Brenner, and R. Mettin, “Bubble size measurements in different acoustic cavitation structures: Filaments, clusters, and the acoustically cavitated jet,” *Ultrason. Sonochem.*, vol. 55, no. May 2017, pp. 383–394, 2019.

[35] O. Louisnard, “A simple model of ultrasound propagation in a cavitating liquid. Part I: Theory, nonlinear attenuation and traveling wave generation,” *Ultrason. Sonochem.*, vol. 19, no. 1, pp. 66–76, 2012.

[36] O. Louisnard, “A simple model of ultrasound propagation in a cavitating liquid. Part II: Primary Bjerknes force and bubble structures,” *Ultrason. Sonochem.*, vol. 19, no. 1, pp. 56–65, 2012.

[37] R. Mettin, “From a single bubble to bubble structures in acoustic cavitation,” in *Oscillations, Waves and Interactions*, T. Kurz, U. Parlitz, and U. Kaatze, Eds. Göttingen: Universitätsverlag Göttingen, 2007, pp. 171–198.

[38] S. A. Suslov, A. Ooi, and R. Manasseh, “Nonlinear dynamic behavior of microscopic bubbles near a rigid wall,” *Phys. Rev. E - Stat. Nonlinear, Soft Matter Phys.*, vol. 85, no. 6, pp. 1–13, 2012.

[39] F. R. Young, *Sonoluminescence*, 1st ed. Boca Raton, FL: CRC Press, 2005.

[40] R. Mettin, T. Nowak, A. Thiemann, C. Cairós, and J. Eisener, “Bubbles as hydrophones,” in: *Fortschritte der Akustik - DAGA*, 2014, DEGA Berlin 2014, pp. 704–705.

[41] R. Mettin, C. Cairós, and A. Troia, “Sonochemistry and bubble dynamics,” *Ultrason. Sonochem.*, vol. 25, no. 1, pp. 24–30, 2015.

[42] U. Parlitz, C. Englisch, C. Scheffczyk, and W. Lauterborn, “Bifurcation structure of bubble osillators,” vol. 88, no. August 1990, pp. 1061–1077, 2014.

[43] W. Lauterborn and T. Kurz, “Physics of bubble oscillations,” *Reports Prog. Phys.*, vol. 73, no. 10, 2010.

[44] Y. B. Zudin, “Analog of the Rayleigh equation for the problem of bubble dynamics in a tube,” *J. Eng. Phys. Thermophys.*, vol. 63, no. 1, pp. 672–675, 1992.

[45] A. R. Klotz and K. Hynynen, “Simulations of the Devin and Zudin modified Rayleigh-Plesset equations to model bubble dynamics in a tube,” *Technical Acoustics/ Tekhnicheskaya Akustika*, pp. 1–15, 2010.

[46] S. Kuhn, personal communication.

[47] D. Fernandez Rivas, L. Stricker, A. G. Zijlstra, H. J. G. E. Gardeniers, D. Lohse, and A. Prosperetti, “Ultrasound artificially nucleated bubbles and their sonochemical radical production,” *Ultrason. Sonochem.*, vol. 20, no. 1, pp. 510–524, 2013.

[48] E. S. Nasibullaeva and I. S. Akhatov, “Bubble cluster dynamics in an acoustic field,” *J. Acoust. Soc. Am.*, vol. 133, no. 6, pp. 3727–3738, 2013.

[49] S. Ihara, “Feasibility of hydrogen production by direct water splitting at high temperature,” *Int. J. Hydrogen Energy*, vol. 3, no. 3, pp. 287–296, 1978.

[50] C. von Sonntag, G. Mark, A. Tauber, and H.-P. Schuchmann, “Advances in Sonochemistry,” in *Advances in Sonochemistry*, vol. 5, T. J. Mason, Ed. Oxford, United Kingdom: Elsevier Science & Technology, 1999, pp. 109–145.

[51] Tandiono, S.-W. Ohl, D. S.-W. Ow, E. Klaseboer, V. V. T. Wong, A. Camattari, and C.-D. Ohl, “Creation of cavitation activity in a microfluidic device through acoustically driven capillary waves,” *Lab Chip*, vol. 10, no. 14, pp. 1848–1855, 2010.

[52] J. Lighthill, *Waves in Fluids*. Cambridge, United Kingdom: Cambridge University Press, 2001.

[53] R. J. Lang, “Ultrasonic Atomization of Liquids,” *J. Acoust. Soc. Am.*, vol. 34, no. 1, pp. 28–30, 1962.

[54] M. Kauer, V. Belova-Magri, C. Cairós, G. Linka, and R. Mettin, "High-speed imaging of ultrasound driven cavitation bubbles in blind and through holes," *Ultrason. Sonochem.*, vol. 48, pp. 39–50, 2018.

[55] B. D. Storey and A. J. Szeri, "Water vapour, sonoluminescence and sono chemistry," *Proc. R. Soc. A Math. Phys. Eng. Sci.*, vol. 456, no. 1999, pp. 1685–1709, 2000.

Graphical abstract

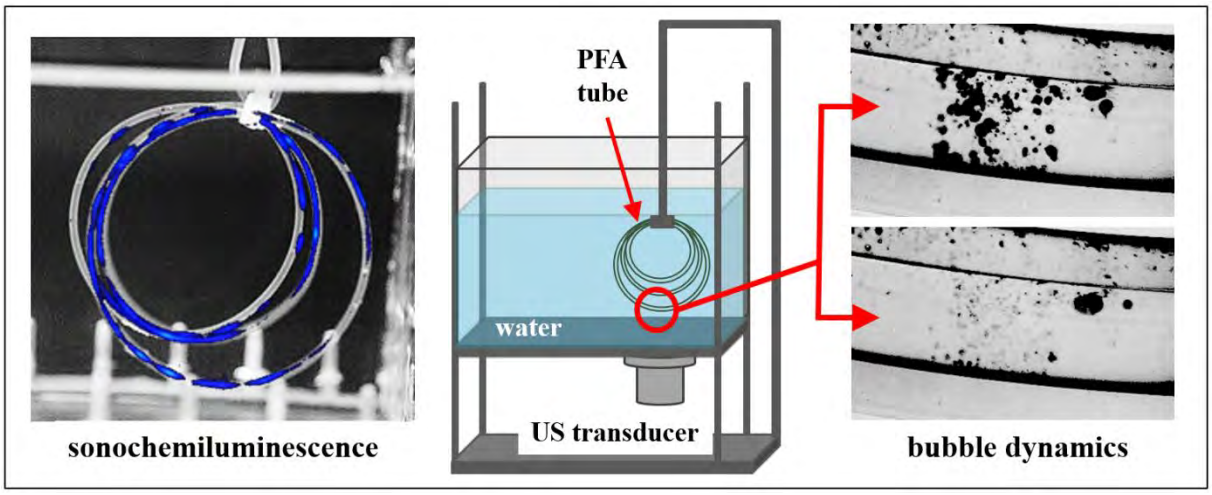

Highlights

- High-speed observation of cavitation bubble structures inside sub-millimeter PFA tubes.
- Bubble nucleation only in water/air slug flow and via entrained gas from the free interface.
- Active bubbles mainly form localized clusters or plugs with the order of 30 – 200 strongly interacting bubbles.
- Sonochemiluminescence recordings and numerical fits of observed bubble dynamics by a modified single bubble model.